Acta Astronautica 201 (2022) 464–471

Contents lists available at ScienceDirect

Acta Astronautica

journal homepage: www.elsevier.com/locate/actaastro

Research paper

Performance improvements of IFM Nano Thruster with highly focused ion beam generated with a compact electrostatic lens module

Nina Sarah Mühlich [a,b,*], Joachim Gerger [a], Bernhard Seifert [a], Friedrich Aumayr [b]

[a] FOTEC Forschungs- und Technologietransfer GmbH, Wr. Neustadt, 2700, Austria
[b] TU Wien, Institute of Applied Physics, Vienna, 1040, Austria

ARTICLE INFO

Keywords:
Beam diagnostics
Electrostatic lens
Electric propulsion
FEEP thruster
Focus electrode
IFM Nano Thruster
Specific impulse
Thrust

ABSTRACT

The requirements for electric propulsion systems suitable for scientific missions are becoming increasingly stringent. This includes, in particular, the reduction of the beam divergence and the alignment accuracy of the thrust vector. Therefore, a modular electrostatic lens module has been developed by using an ion trajectory simulation model which considers the ion produced space charge. The focus module can be mounted on an IFM Nano Thruster with equal side length of 100 mm and it works for the entire operation envelope without increasing the electronics complexity. Experimental beam diagnostics measurements and performance analyses are carried out on an IFM Nano Thruster laboratory model with and without attached focus module. The results show an improvement in thrust and specific impulse of up to 30%. In addition, the beam divergence half-angle is drastically reduced down to $< 20°$ half-angle and a high thrust vector accuracy of $< 0.9°$ is achieved. In addition, the focus module significantly reduces the droplet contamination angle. With this design evolution, the IFM Nano Thruster is becoming a suitable candidate for highly complex scientific missions, such as NGGM.

1. Introduction

Early 2018 the first spacecraft equipped with an IFM Nano Thruster was launched. The thruster has been developed by the research company FOTEC and is commercialised by the space tech company ENPULSION [1,2]. Since then, over 80 IFM Nano Thrusters have been brought into space [3] and the need for electric propulsion constantly increases [4]. The IFM Nano Thruster, shown in Fig. 1 (centre) can be used for a variety of applications, such as attitude control, station-keeping, formation flight, de-orbiting or orbit raising. It is characterised by its compact and modular design suitable for CubeSats (1U). Depending on mission requirements, any number of thrusters can be clustered in various configurations. Due to this wide range of applications, it was desirable to develop an add-on focus module, in order to further increase the thruster's performance. This optimisation should include a reduction of beam divergence and an optimisation of thrust vector stability. With this, the focus module increases the range of achieving thrust and specific impulse and it prevents damage of spacecraft components.

Electrostatic lenses are suitable for focusing a beam of charged particles [5]. For the development of electrostatic lenses, numerical ion trajectory simulation models are particularly suitable, in which a quick parameter variation can be performed [6–10]. A first focus system design for a single needle FEEP thruster was developed at the Austrian Research Center (ARC) in 2005, which was the predecessor of FOTEC. During the design phase it was identified, that a L-shape is appropriate for bending highly divergent ion trajectories [8]. The design resulted in a reduced beam divergence for emission currents up to 300 μA [8]. This geometry is also used for similar ion beam focus systems [7]. Since that time, the single needle emitters have evolved into multiemitters consisting of 28 needles. The shape of the corresponding focus system was similar to the single needle focus system. However, the system has been enlarged, resulting in a bulky and heavy structure with a diameter of 180 mm and 80 mm height [11]. This propulsion system is known as IFM 350 thruster shown in Fig. 1 (left).

In this paper, the focus principle of the IFM 350 is transferred to an add-on module for the significantly smaller IFM Nano Thruster in order to be able to comply with the compact modular design. With a reduction of the focus system, challenges occur, such as an increased space charge. These effects were taken into account by the use of a verified simulation model during the focus module development process [6]. An IFM Nano Thruster laboratory model is experimentally tested with and without attached developed focus module, shown in Fig. 1 (right), using FOTEC's high-precision beam diagnostics system [12]. Under the use of the accurate indirect thrust measurements demonstrated in [13], the

* Correspondence to: TU Wien, Institute of Applied Physics, Vienna, 1040, Austria and FOTEC Forschungs- und Technologietransfer GmbH, Wr. Neustadt, 2700, Austria.
E-mail addresses: muehlich@fotec.at (N.S. Mühlich), gerger@fotec.at (J. Gerger), seifert@fotec.at (B. Seifert), aumayr@iap.tuwien.ac.at (F. Aumayr).

https://doi.org/10.1016/j.actaastro.2022.08.053
Received 19 March 2022; Received in revised form 27 July 2022; Accepted 29 August 2022
Available online 27 September 2022

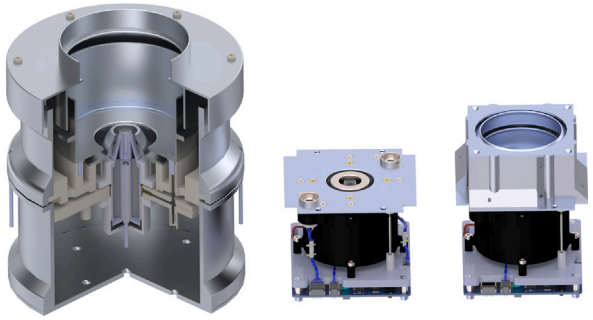

Fig. 1. Evolution of FEEP thruster systems from IFM 350 (left), IFM Nano (centre) and the IFM Nano with attached focus module (right).

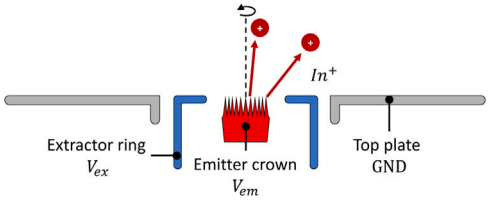

Fig. 2. IFM Nano Thruster electrode geometry and working principle.

performance for different thruster operating points is analysed. With the results presented on beam divergence and thrust vector stability, the thruster is a promising candidate for scientific missions, such as ESA's Next Generation Gravity Mission (NGGM) [14,15].

2. IFM Nano Thruster

2.1. Functional principle

The IFM Nano Thruster is based on decades of development of FEEP technology. The main component of the thruster is a porous tungsten crown consisting of 28 needles wetted with liquid indium. High field strengths are achieved at the needle tips due to the high potential gradient between the emitter crown and the extractor electrode, shown in the schematic drawing in Fig. 2. With this, a so-called Taylor cone builds up on the needle tips from which ions are extracted and accelerated. Due to the use of the capillary forces of liquid metal, no pressurised tanks are required for the propellant storage and feeding. With this method, a compact design of $100 \times 100 \times 82.5$ mm is achieved.

The IFM Nano Thruster is equipped with two thermionic neutralisers, consisting of negatively biased filaments [16]. An electron current corresponding to the ion emission is released in order to prevent a negative charging of the spacecraft.

There are several effects that lead to a defocusing of the thruster ion beam. One of the major source of defocusing is the ion beam's own space charge [17]. Indium ions are released without initial velocity from the nm-sized Taylor cone tip. Due to the slow movement of the ions out of the emitting area, a space charge distribution is formed in front of the Taylor cone tip due to the particle's own charge. The space charge increases the potential in front of the tip, which leads to a widening of the ion beam. The higher the emitter current, the larger the space charge and the greater the beam divergence. At a certain emission current, the potential reaches a size where the ions cannot pass through.

The electrons released by the neutraliser are directed towards the positive space charge in front of the thruster generated by the ion beam. This lowers the positive coulomb potential, which counteracts the beam widening, meaning that the beam is focused using a neutraliser.

It is also known, that the Taylor cone geometry changes with the emission current [18], which is also considered in the simulation model, which will be explained in Section 3.2.

Another defocusing effect comes from the ring-shaped extractor geometry. The emitted ions are accelerated in the direction of the extractor electrode, which leads to an increased divergence of the whole beam.

These defocusing effects can be reduced by means of an electrostatic lens system.

2.2. Performance characterisation

The performance of an electric propulsion system is defined by several parameters, such as thrust, specific impulse and required power. Thrust balances are typically used to determine the thrust directly. Another possibility is the indirect thrust determination by means of beam diagnostics, which works for a FEEP thruster with a high degree of accuracy [13]. Thereby, the thrust T can by calculated with

$$T = I_{em} \cdot \sqrt{\frac{2\ m \cdot V_{em}}{e}} \cdot \gamma, \tag{1}$$

where I_{em} is the emitter current, m/e the mass to charge ratio of the emitted ions, V_{em} the emitter voltage and γ the divergence efficiency. The γ-coefficient considers the beam divergence by including the cosine losses. Typically, the IFM Nano Thruster achieves a thrust ranging from 10–350 μN.

The specific impulse indicates how efficiently the propellant is used:

$$I_{sp} = \frac{1}{g_0} \cdot \sqrt{\frac{2e \cdot V_{em}}{m}} \cdot \eta_m \cdot \gamma, \tag{2}$$

where g_0 is the gravitational acceleration and η_m is the mass efficiency. Tajmar et al. established a model that describes the dependence of the mass efficiency on the emitter current [19]. With increasing emitter current the mass efficiency decreases. Compared to other electric thruster types, the IFM Nano Thruster is characterised by its high specific impulse (2000–6000 s), which is achieved through the high particle velocity determined by V_{em}.

The propulsion system consumes a power of 8–40 W, which is composed of neutraliser consumption, heater power and PPU losses (max. 6 W) as well as beam power $(I_{em} \cdot V_{em})$. The power-to-thrust ratio PTR is another parameter for the performance characterisation of an electric thruster. For a FEEP thruster, the PTR depends on the emitter voltage and the divergence efficiency:

$$PTR = \frac{1}{\gamma} \cdot \sqrt{\frac{e \cdot V_{em}}{2m}}. \tag{3}$$

In addition, the thruster is characterised by the properties of its crown emitter. Emitter crowns are available with different impedances, which define the emission current for a certain voltage applied [16]. Low impedance emitters are suitable for higher thrusts at lower system power. High impedance emitters require an increased power for higher thrusts, but achieve a higher specific impulse.

3. Test setup

3.1. Beam diagnostics

The high precision beam diagnostics system [12] is used to analyse the beam properties of the IFM Nano Thruster laboratory model with and without attached focus module. The beam diagnostics system, shown in Figure Fig. 3, is located in FOTEC's large vacuum facility with a length of 3 m and 2.2 m diameter. Due to the sufficient size of the facility, no noticeable influences on the beam are expected, like charge exchange effects or beam widening due to the facility wall potential. The facility is grounded as well as the thruster housing to reduce the

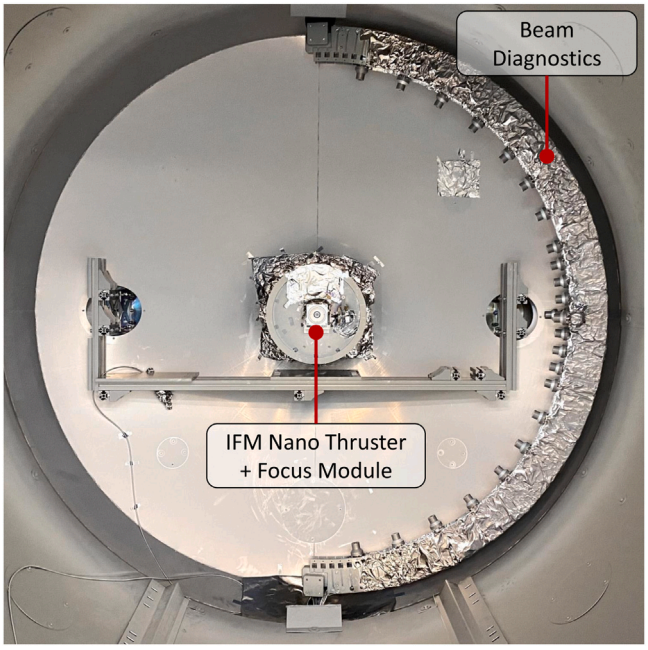

Fig. 3. Test setup of IFM Nano Thruster with attached focus module and rotatable semi-circular beam diagnostics arm equipped with 23 digital Faraday cups.

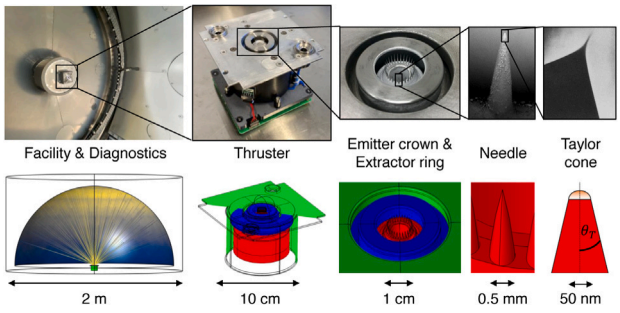

Fig. 4. Experimental setup (top) and implementation in COMSOL ion trajectory simulation model (bottom).[1]

influence of the beam. Due to the low beam density of an IFM Nano Thruster ($\approx 10^{10}$ /m^3 [12]) no neutraliser was used.

The thruster is located in the centre of the rotatable semi-circular diagnostics arm which is equipped with 23 digital Faraday cups (DFCs). In order to obtain a higher resolution of the beam centre, the DFCs are positioned at lower spacing near the geometric centre axis. During a beam scan, the diagnostics arm moves from −80° to +80° in 1° steps at a distance of 90 cm from the emitter crown. The diagnostics system measures the ion current density distribution of the entire beam, from which the main beam properties can be calculated [6,12,13]. This includes the thrust vector and the divergence half-angle, which describes the half-cone angle from the thrust vector that contains 95% of the total beam current. Furthermore, the generated thrust and specific impulse can be computed from the beam profile with high accuracy using Eqs. (1) and (2) [13].

3.2. Simulation model

When developing an electrostatic lens system, there is a large number of possible combinations. An ion trajectory simulation model is suitable for finding the optimal combination with iterative analysis. The model, which is published in [6,20], was set up in COMSOL Multiphysics using the AC/DC and the particle tracing modules. It is based on the experimental setup described in Section 3.1, whereby the test facility including diagnostics system and the IFM Nano Thruster geometry is implemented, as can be seen in Fig. 4. The indium ions are initialised at the nm-sized Taylor cone tip (indicated in orange in Fig. 4) and their trajectories are computed numerically with the electric particle field interaction Multiphysics coupling. The particles ion current density distribution is detected on a half-sphere at a distance of 90 cm diameter, which corresponds to the curved beam diagnostics arm of the experiment. Based on the ion current density distribution, the performance parameters of the thruster can be identically calculated as in the experiment. The model computes the space charge density due to the particle movement through the mesh elements. Furthermore, it considers the change of the Taylor cone geometry according to the emission current by a calibration curve. The Taylor cone geometry is described by the half-cone angle and the jet length, by which the cone is extended. In the model both properties are combined in one parameter θ_T, which is also indicated in the Taylor cone geometry in Fig. 4.

The first calibration of the model in [6,20] is based on the experimental results of a single emitting needle located in the crown emitter EM1. In order to obtain a single needle, the tips of the remaining 27 needles are cut off at the very tip to minimally influence the electric field. In Table 1 the position of the remaining needle inside the crown emitter and the measured ion current density distribution at emission current of 10 µA is shown. Based on the distribution, a divergence half-angle of 23° can be computed for EM1. Further results of the EM1 divergence half-angle depending on the emission current are shown in green in Fig. 5. Measurements were only performed for low emission currents (< 40 µA). The data points show a linear distribution, from which the Taylor cone geometry θ_T was calibrated in [6]

However, the IFM Nano Thruster nominally emits 125 µA per needle. The model was therefore further enhanced on the basis of two additional emitters EM2 and EM3, which is presented the first time within this article. The beam profiles at 10 µA are shown in comparison to EM1 in Table 1. All three profiles have a divergence half-angle of approx. 23–24°. It has to be noted that the utilised emitters are laboratory models used for scientific research.

The divergence half-angle results for EM2 and EM3 at higher emission currents are also presented in Fig. 5. From 0–70 µA the emitters show a linear slope of the divergence half-angle with increasing emission current. From approx. 70 µA, the measurement data saturates and the divergence half-angle increases only slightly. Using the new experimental measurement data of EM2 and EM3, a second calibration curve was established that covers the entire IFM Nano Thruster emission range (< 150 µA per needle) and above. The Taylor cone geometry is thus described with the following updated formula:

$$\theta_T\ [^\circ] = 0.473 + 37.023 \cdot e^{-0.065 \cdot I_{em}\ [\mu A]}, \tag{4}$$

with emitter current I_{em} per needle. More information on simulation model calibration and convergence analysis can be found in [6,20].

Table 1
Experimentally determined single needle beam profiles including divergence half-angle of three different emitters EM1–EM3 at emitter current $I_{em} = 10$ µA.

	EM1	EM2	EM3
Position	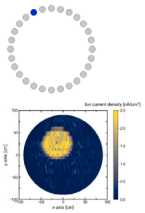	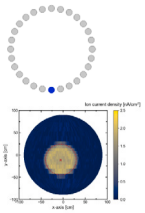	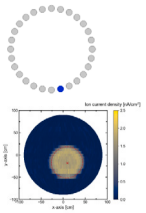
$I_{em} = 10$ µA	$\alpha_{div} = 23.0°$	$\alpha_{div} = 23.1°$	$\alpha_{div} = 23.7°$

[1] Taylor cone picture by Praprotnik [18]

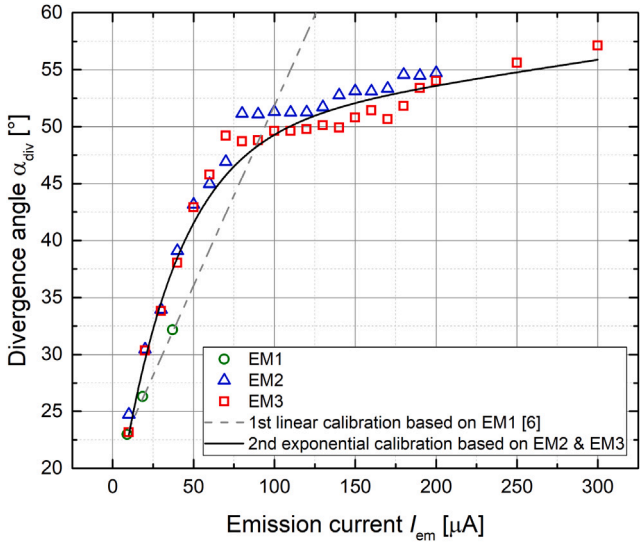

Fig. 5. Experimental divergence half-angle of three different emitters; derived first linear calibration for simulation model based on EM1 and second exponential calibration based on EM2 and EM3.

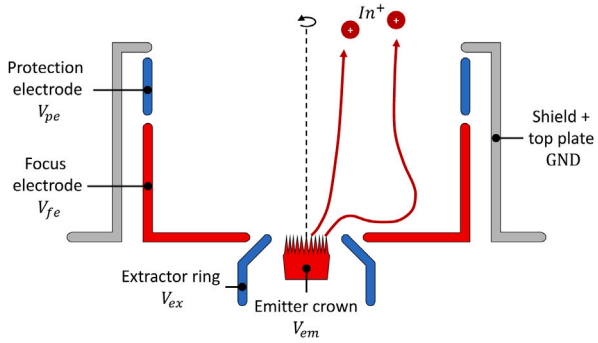

Fig. 6. IFM Nano Thruster electrode geometry with attached focus module.

3.3. Focus electrode module

The developed focus electrode is a stand-alone module that can be attached onto an IFM Nano Thruster and complies with the side length of 100 mm. In order to be able to use the IFM Nano Thruster electronics, the module is supplied with already available potentials.

The ion trajectory simulation model described in Section 3.2 was used to develop the focus module. Thereby, geometric and electrostatic parameters were iteratively varied which ultimately led to the design shown in Fig. 6. The focus module consists of two axial symmetric electrostatic lenses and an electrode shield. It is a typical tube lens consisting of a positive (converging) and a negative (diverging) lens. The converging lens is called focus electrode at potential V_{fe} and the diverging lens is called protection electrode at potential V_{pe}. Based on the previous focus electrode designs, a rotation-symmetrical L-shape is used for the focus electrode, which guides the most divergent beam portions and turns them in direction of the thruster axis [8,9,11,21]. It is at the same potential as the emitter crown $(V_{fe} = V_{em})$. Due to the use of equal potentials, the system can also be classified as an einzel lens.

The protection electrode is at the same negative potential as the extractor $(V_{pe} = V_{ex})$ and is used to create a negative potential in front of the focus electrode. This prevents ambient electrons and electrons released by the neutraliser from entering the focus module, which in turn protects the system from heating up. In addition, the negative potential leads to a further focusing effect. Since $V_{fe} > V_{pe}$, the ions are accelerated while passing through the module. Their velocity is lower in the area of V_{fe} than in the area of V_{pe}, which however leads to a greater focusing than defocusing effect. The grounded shield and top plate are used to shield the high voltage electrodes. Furthermore, it provides a hard limit for Indium droplets.

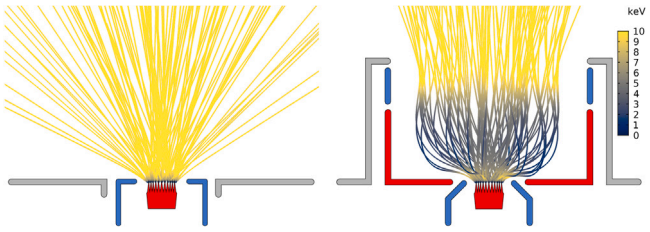

Fig. 7. Simulated ion trajectories of IFM Nano Thruster (left) and with attached focus module (right).

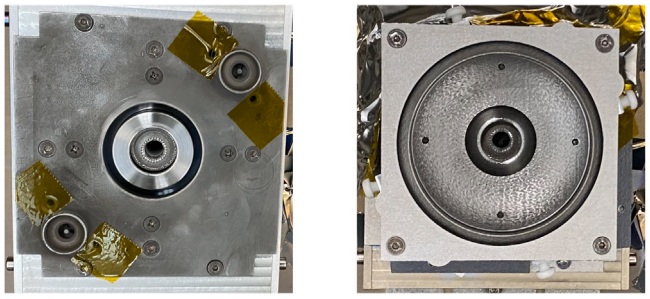

Fig. 8. Close-up view of IFM Nano Thruster laboratory model (left) and with attached focus module (right).

During the development process it was analysed that the aspect ratio of the electrodes is of particular importance. A higher beam focus is achieved by lengthening the tube lenses, which however increase the weight and complexity. Furthermore, it leads to an increased space charge, which may lead to ions trajectories that intersect the extractor electrode.

Further adjustments were carried out in the transfer of the simulation design to a mechanical design. A new extractor geometry was designed to ensure sufficient space for the focus electrode. In addition, the module is equipped with a labyrinth structure to prevent indium droplets from generating a conductive layer on internal insulators. The focus module is attached by replacing the IFM Nano top plate including extractor electrode.

The ion trajectories simulated with the COMSOL Multiphysics simulation model are shown in Fig. 7 for the IFM Nano Thruster compared with attached focus module. The colour of the trajectories indicates the kinetic energy of the ions. The IFM Nano Thruster laboratory model, in close-up view shown in Fig. 8 (left), is supplied with two external high-voltage power supplies. In order to test different potential configurations and measure the current at each electrode, two additional high-voltage power supplies are used to supply the focus module, shown in Fig. 8 (right).

The two IFM Nano Thruster neutralisers were not in operation during the test, since only the pure impact of the focus module had to be investigated. As explained in Section 2.1 the neutralisers would lead to an additional focus effect.

4. Experimental performance measurements

Beam profile measurements were carried out using the setup described in Section 3.1. First, the required voltages at extractor and protection electrode are identified, along the with the total emitted

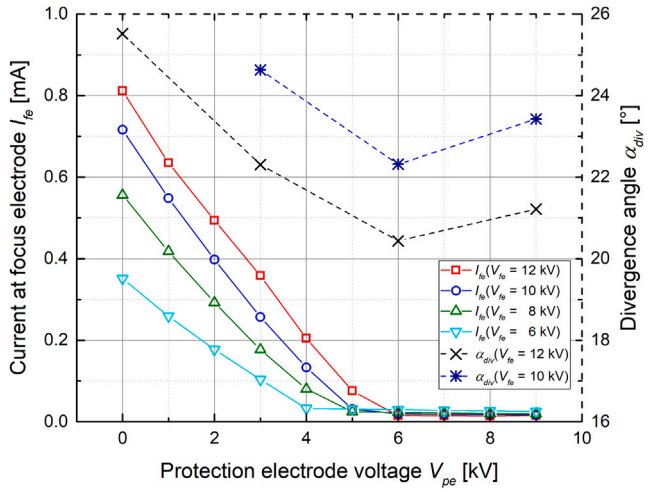

Fig. 9. Measured current at focus electrode I_{fe} at a voltage sweep at the protection electrode V_{pe} for different focus electrode voltages $V_{fe} = V_{em}$.

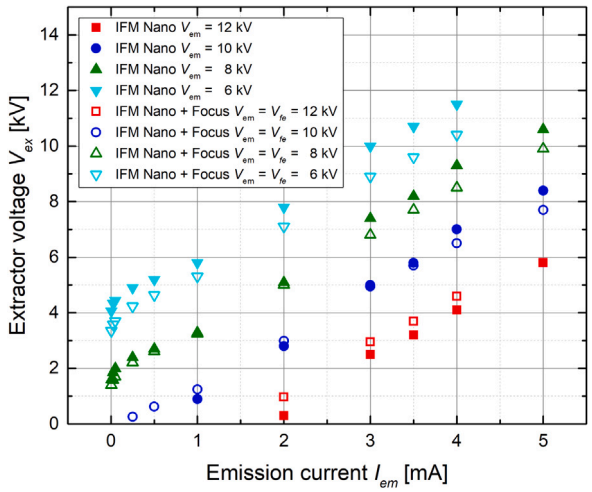

Fig. 10. Required extractor voltage V_{ex} to achieve a certain emitter current I_{em} for different emitter electrode voltages V_{em} with and without attached focus module.

current. In addition, the spherical and 1D beam profile of the IFM Nano Thruster model with and without attached focus module are shown and the key beam properties are analysed. Afterwards, performance analyses are carried out for both systems, including thrust, specific impulse and beam power.

4.1. Determination of operation points

As described in Section 3.3, when a tube lens is lengthened, the space charge can become significant enough to cause ions to be accelerated back towards the extractor electrode. Thus, the ions would not be able to leave the focus module and would not be registered on the diagnostics system. Therefore, the emitted current I_{em} is compared with the measured total beam current I_{tot}, which is computed by integrating the ion current density on the half-sphere detector surface. The measured total currents for both configurations show a maximum variation of 0.2 mA from the emitted current. All deviations are smaller than the experimentally determined accuracy of $< 5\,\%$ of the diagnostics system [13].

In Fig. 9 it is analysed which negative voltage is required at the protection electrode to prevent electrons from outside entering the focus module. For this purpose, a voltage sweep was carried out at the protection electrode V_{pe} and the current at the focus electrode I_{fe} was measured at the same time. The sweep was performed for different focus electrode voltages $V_{fe} = V_{em}$. The higher the voltage at the focus electrode, the higher is the measured current I_{fe}. This means that the higher V_{fe}, the more electrons are attracted. All measurements show that no significant current is measured at the focus electrode above a negative voltage at the protection electrode of $V_{pe} = -6$ kV. Furthermore, in Fig. 9 the divergence half-angle was observed for different protection electrode voltages and two different focus electrode voltages. For both focus voltages the divergence half-angle reaches a minimum at −6 kV. Due to these two reasons, −6 kV is applied to the protection electrode for all measurements.

The required extractor voltage to emit a certain current with and without attached focus module is compared in Fig. 10. The emitter voltage respectively the focus electrode voltage was kept constant $(V_{em} = V_{fe} = \text{const.})$ for each measurement series. The higher the current to be emitted, the higher the required extractor voltage. When a lower emitter voltage is applied, a correspondingly higher extractor voltage is required. When comparing the required extractor voltage with and without focus for $V_{em} = 10$ kV, it can be identified that the value is similar with maximum deviation of 0.7 kV. With lower emitter voltages, a higher extractor voltage is required when using the focus module. However, with a higher emitter voltage, a lower extractor voltage is required by using the focus module. This means that there are no significant differences in required power when using the focus module.

4.2. Beam profile comparison

In order to visualise the beam profiles, the spherically recorded measurement data is projected on Cartesian coordinates. An example of the IFM Nano Thruster test model beam profile at nominal emitter current of 3.5 mA can be seen in Fig. 11 (top). The calculated thrust vector is indicated with a cross and the divergence half-angle with a dashed circle. In this case the calculated thrust vector misalignment is 2.6 ° from the thruster geometric centre. The divergence half-angle amounts to 59.7 °. When comparing the beam profile at the same thruster operation point ($I_{em} = 3.5$ mA, $V_{em} = 12$ kV) with attached focus module, as shown in Fig. 11 (bottom) a drastic reduction of the divergence half-angle by $\approx 40°$ is achieved. The thrust vector misalignment reduces to 0.2° and the divergence half-angle to 20.3°. The profile shows a circular distribution with sharp edges.

In order to be able to examine the structure of the profiles more precisely, the angular ion current density distribution of a horizontal cut through the profiles of Fig. 11 is shown in Fig. 12. The beam profile of the IFM Nano Thruster laboratory module shows a symmetrical distribution, without sharp edges since the individual circular single needle profiles are overlapping. The beam profile generated with the focus module has a steep increase at −23° and a steep decrease at +23°. A parabolic structure ranges from −13° to +13°, which fades into sharp spikes at −18° and +18°. The spikes originate from the ion trajectories that were least affected by the focus module, which was identified with the ion trajectory simulation model. The maximum ion current density in the centre of the profile with attached focus module is six times higher than without. This is due to the fact that the total current is distributed over a significantly smaller area.

4.3. Key beam properties comparison

The beam properties shown visually in the beam profiles of Section 4.2 are analysed in more detail by varying the emitter current and voltage. Fig. 13 shows the divergence half-angle as a function of the emitter current for different emitter voltages. The filled data points represent the results of the beam produced by the IFM Nano Thruster

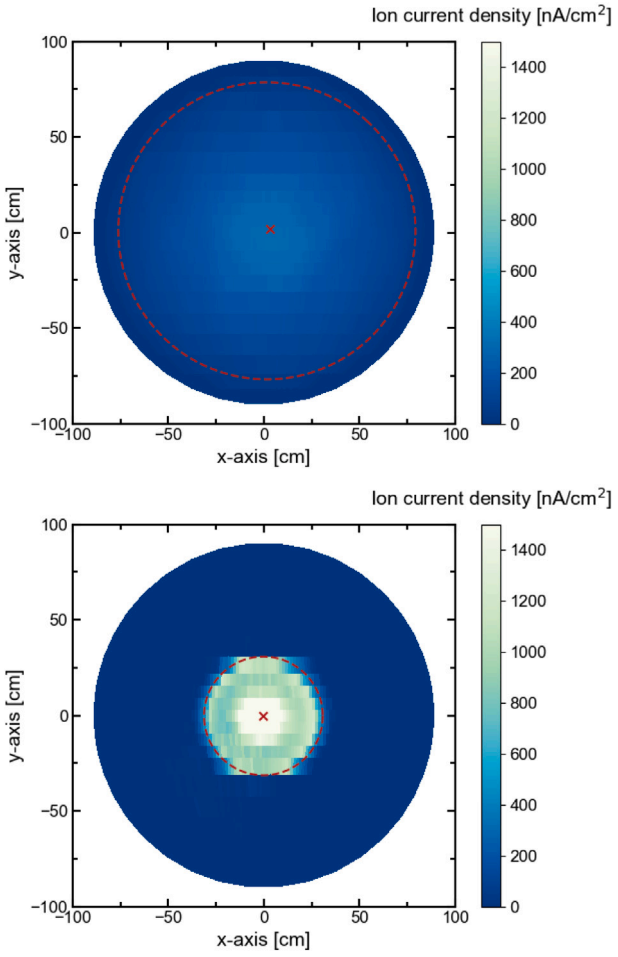

Fig. 11. Beam profile of IFM Nano Thruster laboratory model (top) and with attached focus module (bottom) at emitter current of I_{em} = 3.5 mA and emitter voltage of V_{em} = 12 kV.

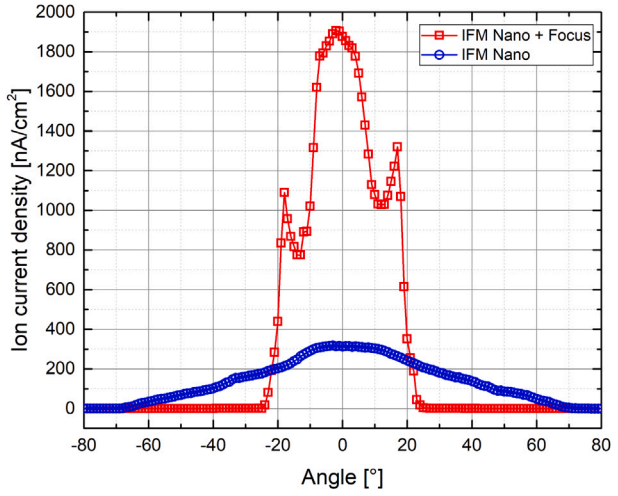

Fig. 12. Angular ion current density distribution at horizontal cut through spherical beam profile for IFM Nano Thruster with and without attached focus module at I_{em} = 3.5 mA and V_{em} = 12 kV.

laboratory model. With increasing emitter current the divergence half-angle increases due to the increased space charge in front of the needle tips, which is described in Section 2.1. Furthermore, the divergence

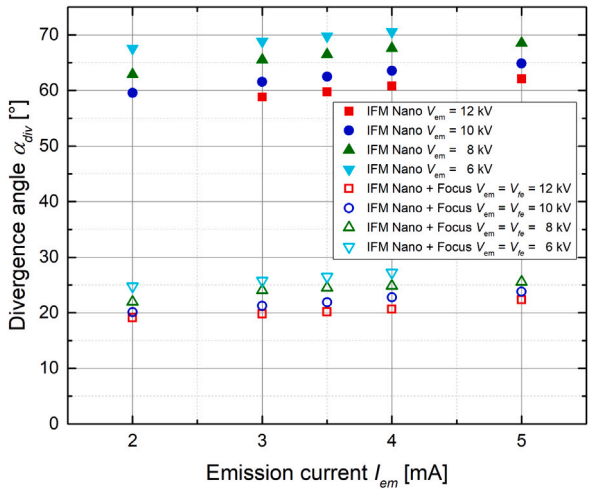

Fig. 13. Divergence half-angle α_{div} as a function of the emitter current I_{em} for different emitter voltages V_{em} for IFM Nano Thruster with and without attached focus module.

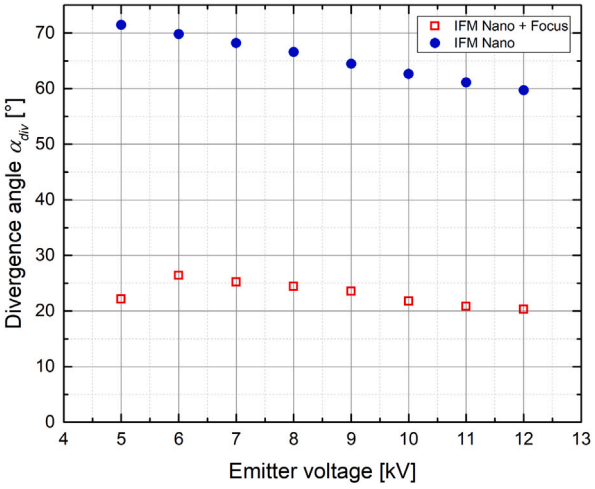

Fig. 14. Divergence half-angle α_{div} as a function of the emitter voltage V_{em} at constant emitter current I_{em} = 3.5 mA for IFM Nano Thruster with and without attached focus module.

half-angle increases with lower emitter voltage and higher extractor voltage respectively. This can be explained with the ring-shaped extractor geometry, which leads to a widening of the beam, also described in Section 2.1. Overall, the divergence half-angle ranges from 59° to 71° for the IFM Nano Thruster laboratory model.

When comparing the results with the unfilled data points of the attached focus module a similar behaviour can be observed which can be attributed to the same explanations. For all operating points, the focus module leads to a reduction of the beam divergence by 41 ± 2.3°. With the use of the focus module, the divergence half-angle ranges from 19° to 27°. In conclusion, the most focused beam is achieved by applying a high emitter voltage and low emitter current.

A further divergence half-angle investigation was carried out in Fig. 14 at constant emitter current I_{em} = 3.5 mA for different emitter voltages. When comparing the results of the IFM Nano Thruster test module with and without attached focus module, it is noticeable that the divergence half-angle decreases linearly with the emitter voltage in both cases. The slope without focus module (m = −1.7) is larger than that with focus module (m = −1.1), calculated for data points from 6–12 kV. The lower slope is caused by the fact that the focus module counteracts the extractor beam widening effect. When looking at the

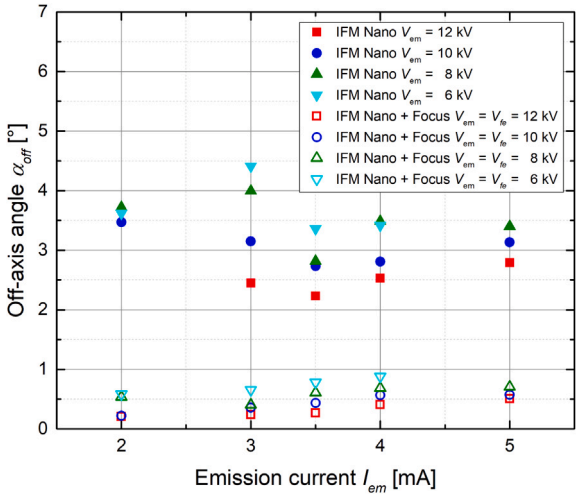

Fig. 15. Off-axis angle α_{off} as function of the emitter current I_{em} for different emitter voltages V_{em} for IFM Nano Thruster with and without attached focus module.

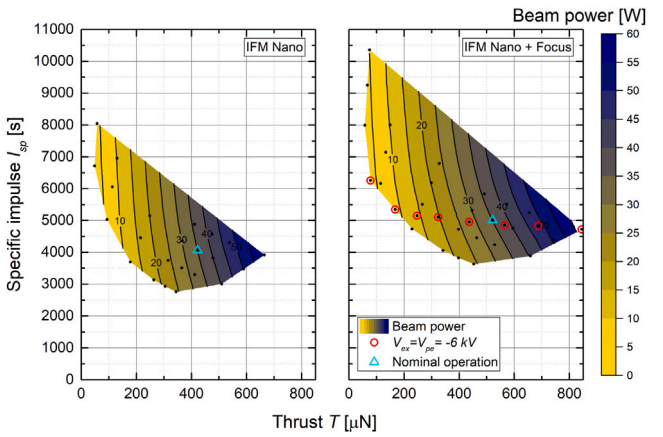

Fig. 16. IFM Nano Thruster laboratory model performance map without (left) and with attached focus module (right).

divergence half-angle with attached focus module, it is noticeable that at the lowest emitter voltage $V_{em} = 5$ kV a re-focusing occurs. As shown in Fig. 6, the most divergent trajectories are most affected by the focus module. This could be an explanation for the more efficiently focusing at the lowest beam power in Fig. 14. In the future, it will be investigated in more detail what occurs at even lower emitter voltages, since then the thruster can be operated with minimum power.

The thrust vector direction can be described with the off-axis angle, which is the angle between the thrust vector and the thruster geometrical centre axis. In Fig. 15 the measured off-axis angle as function of the emitter current for different emitter voltages can be seen. The off-axis angle varies from 2.2 ° to 4.4 °. This deviation from 0 ° can be explained by a slight misalignment between emitter crown and extractor ring during the assembly of the thruster laboratory model. The unfilled data points obtained with the attached focus module show an angle which is always smaller than 0.9 °. This is also the case when emission from some needles ceases at a lower current or if the current is not equally balanced between the needles. This means that the focus module realigns the beam with the geometrical axis of the thruster and therefore compensates slight mechanical inaccuracies during thruster assembly.

4.4. Performance comparison

The performance of an electric propulsion thruster is typically described by a performance map shown in Fig. 16 created for the IFM Nano Thruster laboratory model and with attached focus module. Thrust computations were carried out using Eq. (1) with the divergence efficiency γ calculated from the beam diagnostics measurements. The specific impulse was computed with Eq. (2) using the described mass efficiency model for a tip radius of 2 µm and also the γ-coefficient from the beam measurements. The performance map was generated by varying the emitter current I_{em} and the electrode voltages of emitter V_{em} and extractor V_{ex}. The focus electrode voltage again corresponds to the emitter voltage $V_{fe} = V_{em}$ and the protection electrode was constantly at −6 kV.

When comparing the performance map of the IFM Nano Thruster test model and the focus module in Fig. 16, it is obvious that the performance covers a wider area by using equal beam power. The thrust range increase up to 815 µN compared to 665 µN and the specific impulse ranges from 3600–10300 s compared to 2700–8000 s. Both parameters improve by the same percentage, since voltage and current are included in Eqs. (1) and (2) in the same ratio, whereby in Eq. (2) the current is included in the mass efficiency. Both the thrust and the specific impulse increase by up to 32%. Furthermore, the required power to reach a certain thrust *PTR* decreases with the focus module. When looking at the nominal operation point (cyan) at 35 W it can also be seen that a higher thrust and specific impulse can be achieved. Customised operation is enabled in the entire area of the performance map depending on the available beam power.

The red data points in Fig. 16 (right) are intended to show that the entire thrust range can be covered by using only two HV supplies. Here the extractor voltage was equal to the protection electrode voltage $(V_{ex} = V_{pe} = -6\ \text{kV})$. The thrust was changed by changing the emitter voltage $(V_{em} = V_{fe})$ from 5 to 12 kV in steps of 1 kV. Thereby, the produced thrust is in the upper specific pulse range of an IFM Nano Thruster.

5. Conclusion

An evolutionary focus module for the IFM Nano Thruster was developed, which is consistent with the modular design due to its compact dimensions of 100 × 100 mm and its flexible interchangeability. The module was developed using a verified ion trajectory simulation model. Since the simulation model considers the space charge of the emitting ions, a compact focus design could be developed. With this the height of the IFM Nano Thruster with attached focus module is increased by only 42 mm and by an additional weight of less than 300 g.

Experimental beam diagnostics measurements were carried out to investigate the beam characteristics and performance of an IFM Nano Thruster laboratory model with and without attached focus module. The module achieves up to 30% higher performance, i.e. thrust and specific impulse, with the same available power. In addition, it was demonstrated that the already available two high voltage supplies are sufficient to cover a thrust range up to 800 µN in the upper specific impulse range. This means that the available IFM Nano Thruster electronics can be reused also with attached focus module. Furthermore, it was observed that by using the focus module the beam divergence can be reduced by 41 ± 2.3° to an angle of less than 20°. This allows the IFM Nano Thruster to be competitive with other electrical propulsion systems that can generate highly focused beams, such as gridded ion thrusters. In addition, the thrust vector misalignment from the geometric centre axis was measured, which was for all measurements with focus module below 0.9°. This compensates, for example, the varying emission levels of individual needles or alignment inaccuracies during the assembly. It was also shown that the ion trajectory focusing is effective for all IFM Nano Thruster operating points. With these performance and beam characteristics, the IFM Nano Thruster is a

promising candidate for scientific missions, such as NGGM. Here it is suitable for both required propulsion systems, as main propulsion in a clustered version for drag compensation and as single module for fine attitude control. In the future, the newly developed focus module will be tested for its longevity before it is passed on for commercialisation. Furthermore, the IFM Nano Thruster neutralisers will be integrated at two facing corners of the focus module.

Declaration of competing interest

The authors declare that they have no known competing financial interests or personal relationships that could have appeared to influence the work reported in this paper.

Acknowledgements

This document is the result of research projects funded by the European Space Agency (ESA) under the contract 4000127152/19NL/HB and the Austrian Research Promotion Agency (FFG) under the contract 874844. The authors acknowledge the TU Wien Bibliothek, Austria for financial support through its Open Access Funding Program.

References

[1] B. Seifert, N. Buldrini, T. Hörbe, F. Plesescu, A. Reissner, D. Krejci, P. Friedhoff, S. Lai, In-orbit demonstration of the indium-FEEP IFM nano thruster, in: 6th SPC, Seville, Spain, 2018.

[2] D. Krejci, A. Reissner, B. Seifert, D. Jelem, T. Hörbe, F. Plesescu, P. Friedhoff, S. Lai, Demonstration of the IFM nano feep thruster in low earth orbit, in: 4S Symposium, Sorrento, Italy, 2018.

[3] ENPULSION GmbH, 2022 URL https://www.enpulsion.com/.

[4] D. Lev, R.M. Myers, K.M. Lemmer, J. Kolbeck, H. Koizumi, K. Polzin, The technological and commercial expansion of electric propulsion, Acta Astronaut. 159 (2019) 213–227, http://dx.doi.org/10.1016/j.actaastro.2019.03.058.

[5] J. Orloff, M. Utlaut, L. Swanson, High Resolution Focused Ion Beams FIB and Its Applications, Springer, ISBN: 978-1-4615-0765-9, 2003, http://dx.doi.org/10.1007/978-1-4615-0765-9.

[6] N.S. Mühlich, B. Seifert, F. Aumayr, IFM nano thruster performance studied by experiments and numerical simulations, J. Phys. D: Appl. Phys. 54 (2021) 095203, http://dx.doi.org/10.1088/1361-6463/abc84c.

[7] T. Morris, M. Forget, C. Malardier-Jugroot, M. Jugroot, Multi-scale investigation of a colloid micro-propulsion system, Plasma Processes Polym. 8 (6) (2011) 478–489, http://dx.doi.org/10.1002/ppap.201100003.

[8] I. Vasiljevich, M. Tajmar, N. Buldrini, A. Genovese, K. Marhold, Development of a focus electrode for an indium FEEP thruster, in: 41st JPC, American Institute of Aeronautics and Astronautics, 2005, http://dx.doi.org/10.2514/6.2005-4384.

[9] I. Vasiljevich, M. Tajmar, The beam divergence of an indium LMIS at a distance of 50μm as determined by plasma diagnostic measurements, Ultramicroscopy 111 (8) (2011) 969–972, http://dx.doi.org/10.1016/j.ultramic.2011.01.040.

[10] G. Cai, H. Zheng, L. Liu, X. Ren, B. He, Three-dimensional particle simulation of ion thruster plume impingement, Acta Astronaut. 151 (2018) 645–654, http://dx.doi.org/10.1016/j.actaastro.2018.07.007.

[11] A. Reissner, N. Buldrini, B. Seifert, F. Plesescu, C. Scharlemann, J. González del Amo, Mn-FEEP thruster module design and preliminary performance testing, in: 33rd IEPC, (IEPC-2013-G) 2013.

[12] N.S. Mühlich, B. Seifert, E. Ceribas, J. Gerger, F. Aumayr, High-precision digital faraday cups for FEEP thrusters, J. Instrum. 17 (2022) P08008, http://dx.doi.org/10.1088/1748-0221/17/08/P08008.

[13] N.S. Mühlich, J. Gerger, B. Seifert, F. Aumayr, Simultaneously measured direct and indirect thrust of a FEEP thruster using novel thrust balance and beam diagnostics, Acta Astronaut. 197 (2022) 107–114, http://dx.doi.org/10.1016/j.actaastro.2022.05.009.

[14] L. Massotti, J.G. del Amo, P. Silvestrin, D. Krejci, A. Reissner, B. Seifert, The next generation gravity mission and the qualification of the indium-fed mN-FEEP thruster, CEAS Space J. 14 (1) (2021) 109–124, http://dx.doi.org/10.1007/s12567-021-00386-0.

[15] S. Cesare, M. Aguirre, A. Allasio, B. Leone, L. Massotti, D. Muzi, P. Silvestrin, The measurement of earth's gravity field after the GOCE mission, Acta Astronaut. 67 (7–8) (2010) 702–712, http://dx.doi.org/10.1016/j.actaastro.2010.06.021.

[16] D. Krejci, V. Hugonnaud, T. Schönherr, B. Little, A. Reissner, B. Seifert, Q. Koch, E. Bosch-Borràs, J. González del Amo, Full performance mapping of the IFM nano thruster, including direct thrust measurements, JoSS (2019).

[17] M. Szilagyi, Electron and Ion Optics, Springer US, 1988, http://dx.doi.org/10.1007/978-1-4613-0923-9.

[18] B. Praprotnik, W. Driesel, C. Dietzsch, H. Niedrig, HV-TEM in-situ investigations of the tip shape of indium liquid metal ion emitter, Surf. Sci. (314) (1994) 353–364, http://dx.doi.org/10.1016/0039-6028(94)90237-2.

[19] M. Tajmar, Influence of taylor cone size on droplet generation in an indium liquid metal ion source, Appl. Phys. A: Mater. Sci. Process. (81) (2005) 1447–1450, http://dx.doi.org/10.1007/s00339-005-3207-3.

[20] N.S. Mühlich, B. Seifert, F. Aumayr, Verification of simulation model based on beam diagnostics measurements of the IFM nano thruster, in: 72nd IAC, (IAC-21-C4.6.14) 2021.

[21] D. Jelem, Private communication, 2017.